Influence of length and conformation of saccharide head groups on the mechanics of glycolipid membranes: Unraveled by off-specular neutron scattering

Akihisa Yamamoto,[1,2,a)] Wasim Abuillan,[1] Alexandra S. Burk,[1,3] Alexander Körner,[1] Annika Ries,[4] Daniel B. Werz,[5] Bruno Demé,[6] and Motomu Tanaka[1,2,a)]
[1]*Physical Chemistry of Biosystems, Institute of Physical Chemistry, University of Heidelberg, 69120 Heidelberg, Germany*
[2]*Institute for Integrated Cell-Material Sciences (iCeMS), Kyoto University, Kyoto 606-8501, Japan*
[3]*Institute of Toxicology and Genetics, Karlsruhe Institute of Technology, 76021 Karlsruhe, Germany*
[4]*Institute of Organic and Biomolecular Chemistry, University of Göttingen, 37077 Göttingen, Germany*
[5]*Institute of Organic Chemistry, Technische Universität Braunschweig, 38106 Braunschweig, Germany*
[6]*Institut Laue-Langevin, 38042 Grenoble Cedex 9, Grenoble, France*

(Received 4 November 2014; accepted 6 April 2015; published online 21 April 2015)

The mechanical properties of multilayer stacks of Gb3 glycolipid that play key roles in metabolic disorders (Fabry disease) were determined quantitatively by using specular and off-specular neutron scattering. Because of the geometry of membrane stacks deposited on planar substrates, the scattered intensity profile was analyzed in a 2D reciprocal space map as a function of in-plane and out-of-plane scattering vector components. The two principal mechanical parameters of the membranes, namely, bending rigidity and compression modulus, can be quantified by full calculation of scattering functions with the aid of an effective cut-off radius that takes the finite sample size into consideration. The bulkier "bent" Gb3 trisaccharide group makes the membrane mechanics distinctly different from cylindrical disaccharide (lactose) head groups and shorter "bent" disaccharide (gentiobiose) head groups. The mechanical characterization of membranes enriched with complex glycolipids has high importance in understanding the mechanisms of diseases such as sphingolipidoses caused by the accumulation of non-degenerated glycosphingolipids in lysosomes or inhibition of protein synthesis triggered by the specific binding of Shiga toxin to Gb3. [http://dx.doi.org/10.1063/1.4918585]

I. INTRODUCTION

X-ray and neutron scattering[1–5] from isotropic lipid suspensions have been widely used to gain insight into structural features of biological membranes over multiple length scales as a function of temperature,[6,7] osmotic pressure,[8,9] and the molar ratios of substitutional additives (cholesterol, proteins, etc.).[1,10] However, powder diffraction experiments do not allow for the discrimination of momentum transfers parallel and perpendicular to the membrane planes. In the 1980s, Safinya and co-workers reported the use of planar membrane stacks to geometrically separate specular and off-specular scattering signals.[11,12] Specular signals reflect the inter-membrane potentials between neighboring membranes, while off-specular signals reflect intramembrane structural order, such as pores formed by peptides.[13,14]

Another important application of off-specular scattering is to determine the mechanical properties of membranes, but almost all previous accounts merely dealt with stacks of pure phospholipid membranes.[15,16] As the surface of eukaryotic and prokaryotic cells is coated with saccharide chains that serve as protectors to sustain the structural integrity as well as specific ligands for proteins and complementary saccharides,[17,18] we have previously proposed more realistic model systems based on synthetic and natural glycolipids.[19–21] We demonstrated that the introduction of finite size effects, the so-called "cut-off radius,"[22] allows full calculation of the scattering functions in reciprocal space and quantification of the vertical compression modulus B and the bending rigidity κ of the membranes. We reported that small changes in the molecular structures of the saccharide chains, such as the position and stereochemistry of the glycosidic bonds, significantly influence the mechanical properties of its membrane multilayer.[19] This strategy has been further extended to understand the impact of genetic mutation on the mechanics of membranes composed of bacterial lipopolysaccharides[20] as well as to quantify the physical role of weak saccharide-saccharide interactions in modulating membrane adhesion processes, namely, inter-membrane potentials.[21]

In this account, we physically model the impact of glycolipid on the membrane mechanics which leads to human diseases, such as toxin uptake and metabolic disorders. As a model of glycolipid, we synthesized a lipid with a globotriaose (α-galactose(1-4)-β-galactose(1-4)-β-glucose, Gb3) head group. Gb3 is known as the specific counterpart for

a)Authors to whom correspondence should be addressed. Electronic addresses: ayamamoto@icems.kyoto-u.ac.jp and tanaka@uni-heidelberg.de

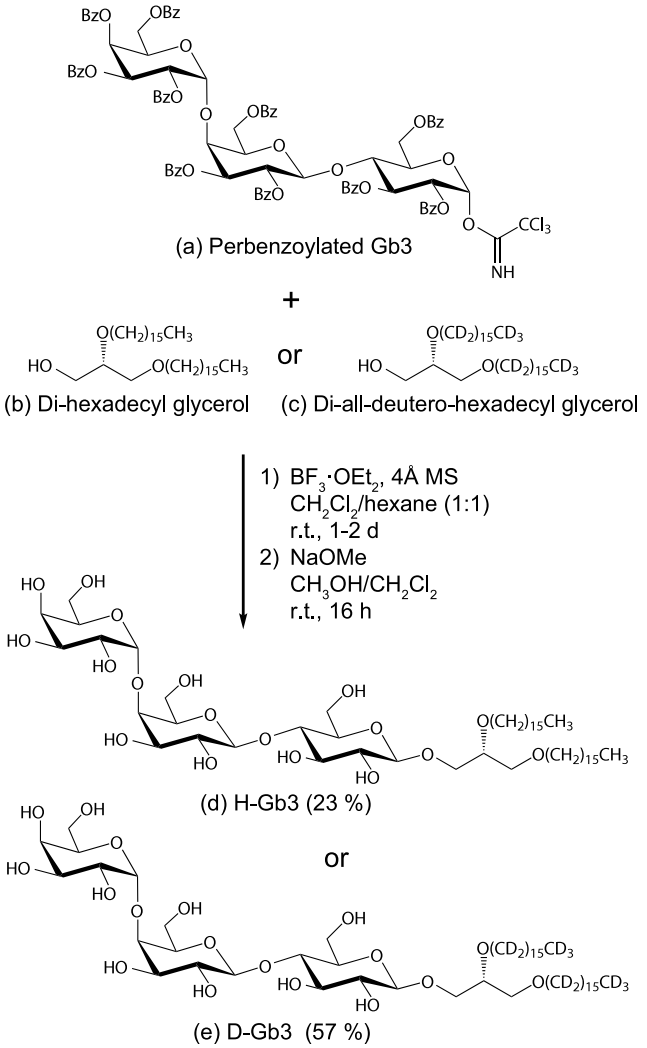

FIG. 1. Chemical synthesis of Gb3 glycolipids with hydrogenated (H-Gb3) and deuterated (D-Gb3) hydrocarbon chains.

verotoxin[23] and Shiga toxin,[24,25] which are highly cytotoxic to the human microvascular endothelium[26] for instance. The A subunit of Shiga toxin has toxic activity leading to the inhibition of protein synthesis, and its B subunit binds specifically to Gb3 oligosaccharide chains. Römer *et al.* reported that the protrusion of large unilamellar vesicles containing Gb3-ceramide molecules was induced by the B subunit of Shiga toxin.[27] Although the induction of negative curvature suggests a major influence on the mechanical properties of cell membranes, there have been no quantitative investigations on the mechanics of membranes enriched with Gb3 lipids. Gb3-ceramide is also known to accumulate in lysosomes, and successively in cellular membrane and other cellular compartments as a result of deficient activity of α-galactosidase, causing a lysosomal storage disorder called Fabry disease.[28,29] Gb3 is assumed to be the main offending molecule that causes Fabry disease, but the influence of its accumulation on the mechanics is still not known.

Here, we assess two principal mechanical parameters, namely, bending rigidity and compression modulus, of Gb3 membrane stacks by using off-specular neutron scattering. Since it is not feasible to fabricate giant unilamellar vesicles of pure Gb3 glycolipids and characterize the mechanics using micropipette aspiration[30] or flicker spectroscopy,[31] multilayers of Gb3 glycolipids deposited on a planar substrate were utilized as one of the simplest but most straightforward experimental systems for highlighting how Gb3 glycolipids influence the principal mechanical properties of membranes. To maximize the contrast of scattering length density under hydration with D_2O and H_2O, we used dihexadecylglycerol anchors with fully hydrogenated and deuterated chains (Fig. 1), respectively. To discuss the influence of carbohydrate head groups on structure and mechanics, the obtained results were systematically compared first with the corresponding values of other glycolipids possessing head groups with slightly different chemical structures (Figs. 2(b) and 2(c)), and further with those of a reference phospholipid, dipalmitoylphosphatidylcholine (DPPC), possessing a saturated dihexadecyl chain (Fig. 2(a)) in order to examine the impact of Gb3 moiety on the membrane mechanics. Details of the obtained results are described in Secs. II–IV.

II. MATERIAL AND METHODS

A. Synthesis of Gb3 glycolipids

Globotriaose derivatives H-Gb3 and D-Gb3 were synthesized using Schmidt glycosylation chemistry.[32] In the first step, the globotriaosyl trichloroacetimidate donor was synthesized. Using standard carbohydrate protecting group chemistry,[33,34] bare Gb3 was perbenzoylated, followed by anomeric deprotection and trichloroacetimidate formation.[35] In the following glycosylation reaction, globotriaosyl trichloroacetimidate (Fig. 1(a)) and either 1,2-di-*O*-hexadecyl-*sn*-3-glycerol (Fig. 1(b)) or 1,2-di-*O*-all-deutero-hexadecyl-*sn*-3-glycerol (Fig. 1(c)) were coupled using $BF_3 \cdot OEt_2$ as promoter.[32] Benzoyl protecting groups were absolutely necessary to avoid intermolecular acyl migration during the glycosylation reac-

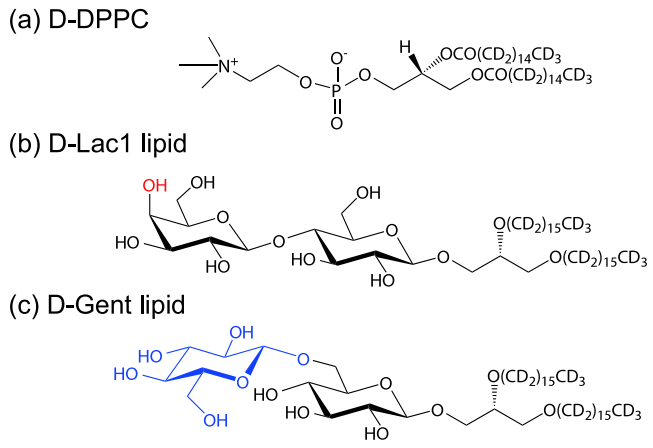

FIG. 2. Chemical structures of (a) D-DPPC, (b) D-Lac1 lipid, and (c) D-Gent lipid, in which the hydrocarbon chains are fully deuterated. D-Lac1 differs from D-Gb3 by the missing third monosaccharide unit which is attached to the hydroxyl group shown in red. D-Lac1 and D-Gent are both disaccharides but reveal different types of glycosidic linkages. The second monosaccharide of D-Gent is connected via the 6-hydroxyl group leading to a "bent" structure, whereas in D-Lac1, it is connected via the 4-hydroxyl group leading to a more cylindrically shaped disaccharide.

tion. After global deprotection under Zemplén conditions,[36] the desired globotriaose derivatives H-Gb3 (Fig. 1(d)) and D-Gb3 (Fig. 1(e)) were obtained. Details of the synthesis, chemical structures, and ^{1}H- and ^{13}C-NMR spectra of the obtained lipids as well as intermediate products are shown in supplementary material (Figs. S1–S12).[37]

B. Materials, sample preparation

The glycolipids were dissolved in 7:3 mixtures (v/v) of chloroform and methanol at a concentration of 2 mg/ml. 1 ml of this solution was deposited onto Si(100) substrates (55 mm × 25 mm) with native oxide (Si-Mat, Landsberg/Lech, Germany). The silicon substrates were cleaned in advance using the modified RCA cleaning method:[38] these wafers were cleaned by successive ultrasonication in acetone, ethanol, and methanol, and subsequently immersed in a solution of 1:1:5 (v/v/v) H_2O_2 (30%)/NH_4OH (30%)/water at 60 °C for 30 min. During the organic solvent evaporation process, Gb3 glycolipids self-assemble into planar membrane stacks owing to their amphiphilic property, aligned parallel to the substrate surface. To remove residual solvent, the wafers were stored at 70 °C for 3 h and then subsequently in a vacuum chamber overnight. Depending on the amount of deposited solution and coated area, the average number of membranes in the stacks was on the order of hundreds.[19] The samples were then stored at 4 °C overnight prior to the measurements to remove the thermal history.

C. Neutron scattering experiments

Specular and off-specular neutron scattering experiments were carried out at ILL D16 (Grenoble, France).[39] As illustrated in Fig. 3, the incoming neutron beam reaches the sample through an aluminum window in the sample chamber, and the angle of incidence Ω is adjusted by using a rotating stage. The beam width was 2 mm horizontally and 25 mm vertically. The scattered beam was detected at exit angle Γ by a position sensitive ^{3}He 2D detector with 128 × 128 channels. The sample was rotated stepwise with respect to the incident beam. At each angle of incidence Ω, the detector readout was normalized to the intensity of the incident beam (using an in-beam monitor), the channel sensitivity, and the illuminated sample area. Next, the 2D detector readout was integrated in the vertical direction, which results in a one-dimensional intensity projection as a function of the horizontal detector channel position (corresponding to Γ). Thus, one Ω scan yielded the recorded intensity as a function of Ω and Γ. As shown in Fig. 3, scattering vector components parallel and perpendicular to the sample planes, q_z and $q_{\|}$, can simply be given by geometric considerations,

$$q_z = \frac{2\pi}{\lambda_n}\left(\sin\left(\Gamma - \Omega\right) + \sin\left(\Omega\right)\right) \tag{1}$$

and

$$q_{\|} = \frac{2\pi}{\lambda_n}\left(\cos\left(\Gamma - \Omega\right) - \cos\left(\Omega\right)\right), \tag{2}$$

where λ_n is the wavelength of incoming neutron beam (λ_n = 4.75 Å, $\Delta\lambda_n/\lambda_n$ = 1%).

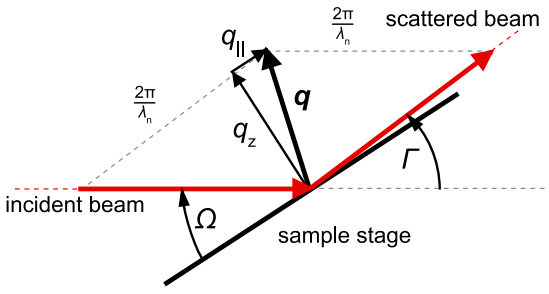

FIG. 3. Experimental scattering geometry. Membrane multilayer of H-Gb3 or D-Gb3 is mounted on the rotating sample stage with the sample plane parallel to the stage. Reciprocal vector components q_z and $q_{\|}$ are obtained from the angle of incidence Ω and scattered angle Γ in accordance with Eqs. (1) and (2).

D. Sample environment

ILL provides a climate chamber in which the temperature and relative humidity are regulated[19] which consists of two thermally isolated but interconnected cells for vapor exchange. The temperatures in the sample chamber T_s and water reservoir T_r are regulated by thermostats (Phoenix II, Haake, Karlsruhe, Germany. ΔT = 0.1 °C) to control the sample temperature (40 °C and 60 °C) and hence the relative humidity h_{rel} (~ 60% and ~ 95%). The osmotic pressure exerted on the sample is defined by the chemical potential of water vapor in equilibrium. According to van't Hoff's law, the osmotic pressure[40] p_{osm} is given by

$$p_{osm}\left(T_r\right) = -\frac{k_B T_s}{V_{water}} \ln\left[h_{rel}\left(T_r\right)\right], \tag{3}$$

where V_{water} is the molecular volume of water, k_B is the Boltzmann constant, and h_{rel} is the relative humidity which is given as a function of T_s and T_r as

$$h_{rel}\left(T_r\right) = p\left(T_r\right)/p\left(T_s\right), \tag{4}$$

where $p\left(T_s\right)$ and $p\left(T_r\right)$ denote the saturation water vapor pressures in the sample and reservoir chambers, respectively (T_r = 10 °C and T_s = 40 °C, T_r = 32 °C and T_s = 60 °C for h_{rel} ~ 60%, and T_r = 38 °C and T_s = 40 °C, T_r = 58 °C and T_s = 60 °C for h_{rel} ~ 95%, respectively). At thermal equilibrium, the disjoining pressure counterbalances the osmotic pressure.[18,41] For the measurements in bulk buffers,[19,20] a self-built liquid cell consisting of two Si wafers with a gap of 0.17 mm was used. To guarantee that the sample reaches the equilibrium state, the sample was held at each temperature and humidity condition for at least 90 min before measurement.

III. FULL CALCULATION OF SCATTERING SIGNALS

Within the framework of a continuum model approximation, the total free energy of membrane stacks can be described using the discrete smectic Hamiltonian[22] H,

$$H = \int d^2r \left\{\sum_{n=1}^{N-1}\left(\frac{B}{2d}(u_{n+1} - u_n)^2 + \frac{\kappa}{2}\left(\nabla^2 u_n\right)^2\right)\right\}, \tag{5}$$

where N is the total number of membranes, d is the average lamellar equilibrium periodicity, and u_k is the out-of-plane displacement of the kth membrane from its average position $\langle u_k \rangle$. The vertical compressibility of the membrane stacks is characterized by the compression modulus B, and the resistance of the membranes against bending is characterized by the bending rigidity κ. The scattering signals were modeled within the framework of a kinematic approximation, which assumes that the intensity of the scattering beam is much weaker (more than a factor of thousand) than the incident beam, that is, the incident angle Ω is well above the critical angle.[42] It should be noted that the 1st Bragg sheet does not fulfill the requirement from this assumption in our experimental systems.

The scattering intensity from periodic membrane stacks possessing correlated roughness can be expressed as[43]

$$S(q_z, q_\parallel) \propto \frac{1}{{q_z}^2}\left[N\int_{-\infty}^{\infty}\exp\left(-{q_z}^2 g_0(r)/2\right)\exp\left(-iq_\parallel r\right)dr + 2\sum_{k=1}^{N}(N-k)\cos(kq_z d) \times \int_{-\infty}^{\infty}\exp\left(-{q_z}^2 g_k(r)/2\right)\exp\left(-iq_\parallel r\right)dr\right]. \quad (6)$$

Here, the membrane correlation function $g_k(r)$ can be expressed in terms of the de Gennes parameter λ and Caillé parameter η as[22]

$$g_k(r) = \frac{d^2}{\pi^2}\eta\int_{2\pi/R}^{\infty}\frac{1 - J_0(q_\parallel r)\, e^{-\lambda k {q_\parallel}^2 d}}{q_\parallel\sqrt{1 + \frac{\lambda^2 d^2}{4}{q_\parallel}^4}}dq_\parallel, \quad (7)$$

where

$$\eta = \frac{\pi k_B T}{2d^2\sqrt{\kappa B/d}} \quad (8)$$

and

$$\lambda = \sqrt{\kappa/Bd}. \quad (9)$$

J_0 stands for the Bessel function of the first kind, $k = 0$ corresponds to the membrane self-correlation function and $k > 0$ to the cross-correlations between different membranes, and R represents the effective cut-off radius reflecting the finite sample size that we introduced in our previous works.[19,22] This sets an upper limit on the wavelength of the membrane fluctuations, which corresponds to the sample size.

The Bragg sheet is represented by profiles of (i) the Γ-integrated Bragg sheet intensity and (ii) the Γ width of the sheets. These representations are simultaneously calculated and computed in angular coordinates in order to maintain a uniform grid of data points.[48] The best combination of de Gennes parameter λ and Caillé parameter η from the scattering function analysis yields both compression modulus B and bending rigidity κ from Eqs. (8) and (9). Instrumental resolution was included by convolution of the signal in the Ω and Γ directions with a Gaussian function derived from the finite angular width and spreading of the wavelength.[22]

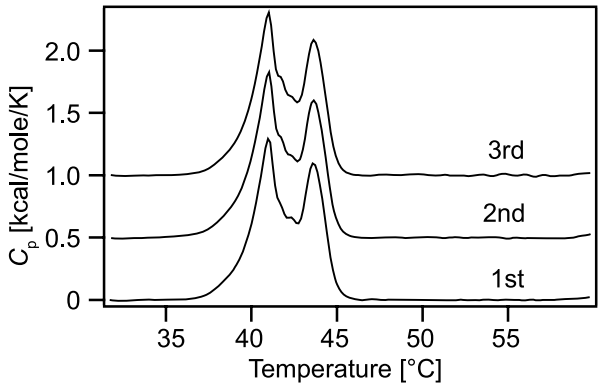

FIG. 4. Differential scanning calorimetry of D-Gb3 suspension recorded at a heating rate of 10 °C/h yielding a main transition enthalpy of $\Delta H = 4.7$ kcal/mol. Successive heating scans exhibited no hysteresis. Each of the scan is separated by an offset of 0.5 kcal/mol/K in a vertical direction for the clarity.

IV. RESULTS AND DISCUSSIONS

Before the scattering experiments, we determined the thermotropic phase transition of Gb3 by using differential scanning calorimetry (DSC), yielding two neighboring endothermal peaks at 40.6 °C and 43.6 °C, with a total enthalpy of $\Delta H = 4.7$ kcal/mol (Fig. 4). The multiple endothermic peaks observed in heating scans suggest polymorphic behavior of lipids, as in other reported glycosphingolipid systems.[44] This enthalpy value is significantly suppressed compared to that of H-Lac1 lipid ($\Delta H_{\text{H-Lac1}} = 30$ kcal/mol),[3] which can be attributed to the shift of the hydrophilic/hydrophobic balance and the entropic contribution caused by the additional α-galactose attached to the 4th position.

Figs. 5(a) and 5(b) show the scattering signals from H-Gb3 and D-Gb3 multilayers at 60 °C and $h_{\text{rel}} \sim 95\%$ in reciprocal coordinates, respectively. Clear specular peaks at $q_\parallel = 0$ and Bragg sheets parallel to the $q_\parallel$ axis indicate the parallel alignment of membranes to planar substrates. An enlarged view of the off specular signal around the 3rd Bragg sheet from D-Gb3 (Fig. 5(b)) is shown in Fig. 5(c). It is notable that the 2nd Bragg peak is less pronounced than the 3rd Bragg peak, which can be attributed to the form factor corresponding to the scattering length density profile. Moreover, the signals from H-Gb3 hydrated in D_2O were much poorer than those from D-Gb3 in H_2O. Hence, the 3rd Bragg sheets of D-Gb3 were mainly used for off-specular analysis to determine the mechanical properties of membranes in the following.

Fig. 6 shows the specular signal intensity obtained from D-Gb3 in 60 °C and $h_{\text{rel}} \sim 95\%$, obtained by integration in the region satisfying $|q_\parallel| < 0.5 \times 10^{-4}$ Å (indicated by dashed lines in Fig. 5(b)). The equilibrium distance between two neighboring bilayers was determined to be $d = 62.6$ Å from two neighboring Bragg peaks.[49] The lamellar periodicity d of membrane multilayers can be expressed as a sum of sublayer thicknesses,

$$d = 2(d_c + d_h) + d_w, \quad (10)$$

where d_c and d_h are the thicknesses of alkyl chains and the headgroup of monolayer, respectively, and d_w is the thickness of the water layer between two neighboring membranes.

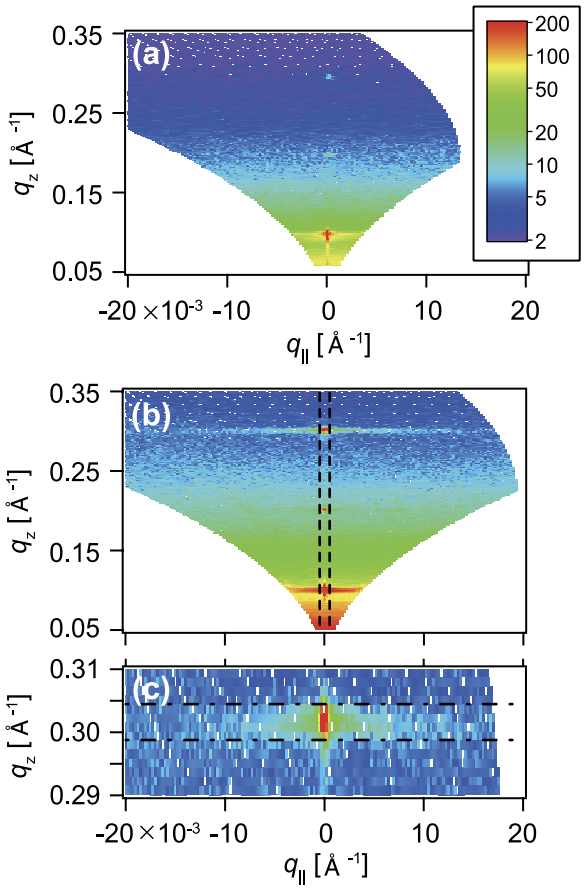

FIG. 5. Scattering intensity from membrane multilayer consisting of (a) H-Gb3 and (b) D-Gb3, and (c) 3rd Bragg sheet of D-Gb3, measured in 60 °C and $h_{rel} \sim 95\%$, shown in a reciprocal space map. The 3rd Bragg sheet is clearly achieved in D-Gb3, whereas it is not identifiable in H-Gb3. The color scale represents the intensity (a.u.) in a log scale. For comparison, the same color scale is used in all of the panels. Data points surrounded by dashed lines in Fig. 5(b) and dashed-dotted lines in Fig. 5(c) are integrated for specular (Fig. 6) and off-specular (Fig. 7(a)) analysis.

Taking d_c as the value of Lac1 in the Lα-phase, which has the same hydrocarbon chains and glycerol junction, of $d_c \sim 16$ Å,[3] the hydrophobic membrane thickness of a bilayer becomes $d_c \sim 32$ Å. Since this is close to half of the lamellar periodicities among the conditions investigated, the contribution from the 2nd mode of Fourier series expansion

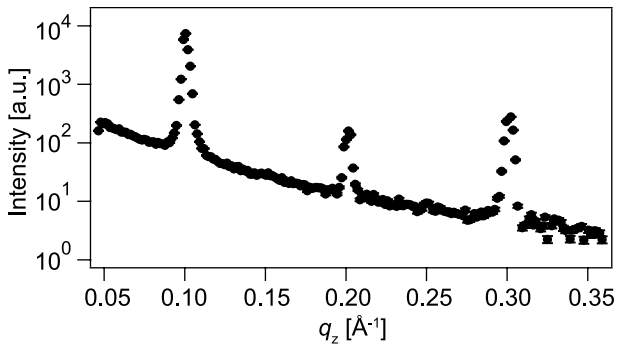

FIG. 6. Intensity profile of specular scattering along $q_{||} = 0$ from D-Gb3 in 60 °C and $h_{rel} \sim 95\%$. Bragg peaks from 1st to 3rd are clearly achieved. A membrane periodicity in the equilibrium state of $d = 62.6$ (Å) is obtained.

can be significantly suppressed to express the scattering length density profile perpendicular to the sample plane, resulting in a weak 2nd Bragg peak.

The effect of two thermodynamic variables on interactions between neighboring membranes was also studied. To investigate the influence of temperature, we performed experiments at 40 °C and 60 °C, below and above the main transition temperature, respectively, while the influence of the osmotic pressure (and thus the disjoining pressure) exerted on the membranes was investigated at a low relative humidity ($h_{rel} \sim 60\%$, $P_{osm} \sim 7.5 \times 10^7$ Pa), high relative humidity ($h_{rel} \sim 95\%$, $P_{osm} \sim 8.0 \times 10^6$ Pa), and in bulk water ($P_{osm} \sim 0$ Pa). Although many of the off-specular scattering signals were too weak for statistically reliable analyses (Fig. S13[37]), the specular Bragg peaks were sufficiently detectable to determine the lamellar periodicity d in all conditions (Fig. S13, inset in each reciprocal space maps[37]). It should be noted that a clear change in the lamellar periodicity could be observed between 40 °C and 60 °C independent of the osmotic pressure. A distinct decrease in the periodicity increasing temperature ($\Delta d = 3$–12 Å) can be attributed to the first order melting transition of alkyl chains, which coincides with the DSC results. Our experimental conditions correspond to the pressure regime where the membrane-membrane interaction is dominated by hydration repulsions[45] that decay exponentially over distance,

$$P_{hydr} \sim \exp\left(-\frac{d}{\lambda_{hydr}}\right), \tag{11}$$

where λ_{hydr} is the characteristic decay length. We found that the obtained values $\lambda_{hydr}^{H-Gb3} = 2.6$ Å and $\lambda_{hydr}^{D-Gb3} = 2.5$ Å are clearly larger than those of H-Gent lipid ($\lambda_{hydr}^{H-Gent} = 0.35$ Å) and H-Lac1 lipid ($\lambda_{hydr}^{H-Lac1} = 0.60$ Å),[19] whereas they are comparable to those reported for phosphocholine membranes ($\lambda_{hydr}^{PC} \sim 2$ Å).[8,44] This finding implies that the membrane-membrane interaction is suppressed by the bulky Gb3 head groups.

Fig. 7 shows the experimental results (symbols) and the corresponding data fittings (red lines) of the 3rd Bragg sheet profile from D-Gb3 membranes measured at 60 °C and $h_{rel} \sim 95\%$. Two profiles were selected for comparison of the experimental data with the data fitting:[50] the intensity profile integrated in Γ direction[51] as a function of $q_{||}$ (Fig. 7(a)) and the width of the 3rd Bragg sheet along Γ as a function of $q_{||}$ (Fig. 7(b)). The signals near the Yoneda wings were not included in the comparison[15] because the first Born approximation becomes invalid when the scattering angle is close or equal to the critical angle due to multiple refractions and reflections. The best matching parameters corresponding to the data fitting are presented in Table I. Note that the cut-off radius R, corresponding to the finite size of the sample, was found from the data fitting to be 1.8 μm, which is in good agreement with the values reported in our previous studies.[19–21] The best fit results (Fig. 7, red lines) yielded $\lambda = 12$ Å and $\eta = 1.8 \times 10^{-2}$, corresponding to $\kappa = 17\ k_BT$ and $B = 8.4$ MPa according to Eqs. (8) and (9).

To highlight the impact of molecular structure such as the number of saccharide units and the type of glycosidic bonds on the mechanical properties of the membrane,

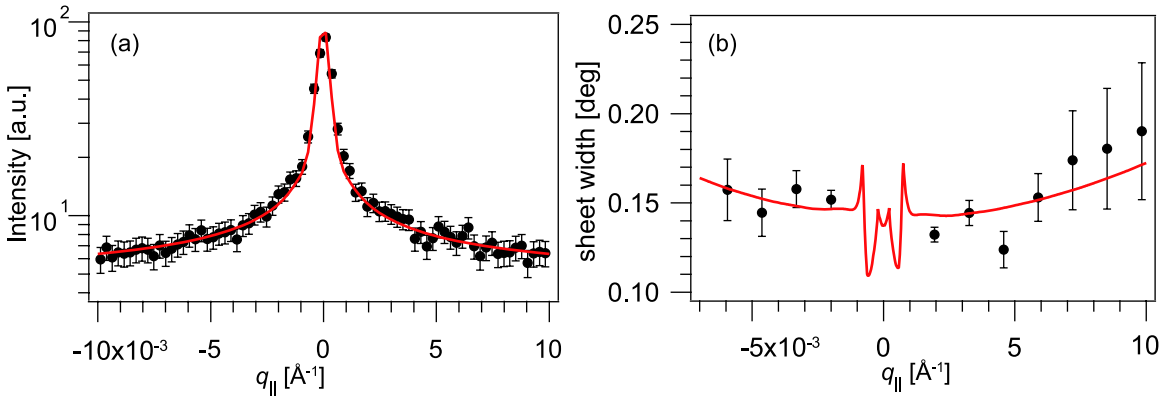

FIG. 7. (a) Intensity and (b) width profile of 3rd Bragg sheet from D-Gb3 measured at 60 °C, $h_{rel} \sim 95\%$. Sheet width as a function of $q_{\|}$ is defined as the FWHM of the Gaussian fit along Γ direction. Red curves represent the best fit to the experimental plot, calculated from Eq. (6) with the parameter set of $\lambda = 12$ Å, $\eta = 1.8 \times 10^{-2}$, which corresponds to $\kappa = 17\ k_BT$ and $B = 8.4$ MPa. Note that the presence of local peaks near $q_{\|} = 0$ is due to the interference of specular signals which does not perpendicularly cross to Bragg sheet in an angular coordinate. This region is not considered for the fitting to experimental data.

we systematically compared the mechanical properties of D-Gb3 with those of other synthetic lipids and glycolipids with different saccharide units (Table II).[19–21] B reflects the sharpness of the inter-membrane interaction potential that determines membrane confinement, while κ reflects the intramembrane interaction between Gb3 glycolipid molecules. For systematic comparison, all the values presented here are obtained from molecules whose hydrophobic chains are fully deuterated dihexadecyl chains in the fluid Lα phase.

First, we compared the mechanical properties of D-Gb3 with D-Lac1, which is lacking only one α-galactose at the 4th position. The attachment of one galactose resulted in a significant decrease in both B and κ. $B_{D-Gb3} = 8.4$ MPa is about half of $B_{D-Lac1} = 17$ MPa, suggesting a significant softening of inter-membrane potential due to the higher degree of hydration caused by the presence of one additional monosaccharide unit. Moreover, $\kappa_{D-Gb3} = 17\ k_BT$ is almost half of $\kappa_{D-Lac1} = 32\ k_BT$, suggesting that Gb3 membrane is less resistant against bending deformation due to the "bent" structure of the trisaccharide head group. This interpretation is supported by the comparison with the corresponding values of D-Gent ($\kappa_{D-Gent} = 8\ k_BT$). Gent lipid also has a "bent" disaccharide head group but the projected length normal to the membrane plane is shorter compared to Gb3. $B_{D-Gent} = 21$ MPa is comparable to B_{D-Lac1} and thus almost double B_{D-Gb3}, suggesting that the confinement of inter-membrane potential is predominantly influenced by the total length of the saccharide head group. The larger compression modulus means that membranes are more vertically correlated, since the membrane displacement u_k can more strongly influence its neighboring layer due to the stronger vertical interaction. The difference between $\kappa_{D-Gent} = 8\ k_BT$ and $\kappa_{D-Gb3} = 17\ k_BT$ could also be attributed to the difference in the length of the saccharide head group.[20] In contrast, the more pronounced difference between κ_{D-Gent} and $\kappa_{D-Lac1} = 32\ k_BT$ can instead be interpreted in terms of the decrease in intra-membrane interactions between the head groups caused by the entropic contribution derived from less ordered lateral packing due to their "bent" structure, which could be identified from a clear difference in T_m; $T_m^{Lac1} = 74$ °C and $T_m^{Gent} = 45$ °C.[3,19]

Second, the mechanical parameters of D-Gb3 membranes were compared with DPPC membranes measured under identical conditions (60 °C, $h_{rel} \sim 95\%$).[21] The compression modulus of D-DPPC $B_{D-DPPC} = 48$ MPa is more than 5-fold that of D-Gb3. Although the comparison under osmotic pressure (and thus not in the presence of bulk water) must be discussed carefully, the significant difference observed here suggests a distinct contribution of saccharide groups to inter-membrane interactions. The distinct difference in compression modulus can be attributed to the presence and absence of bulky trisaccharide head groups. However, it is notable that the bending modulus of D-DPPC $\kappa_{D-DPPC} = 18\ k_BT$ is almost identical to that of D-Gb3. The comparable bending rigidity values obtained here suggest a counter balance to the entropic contribution by intra-membrane interactions between "bent" saccharides that tend to soften the membranes against bending and the thickening of membranes by the elongation of saccharide head groups that tend to increase the bending stiffness of the membranes.

The obtained results clearly demonstrate that the combination of tailored glycolipids and off-specular neutron scattering is a powerful tool for sensitively investigating the

TABLE I. Parameters of the best matching profile obtained by data fitting for D-Gb3 membranes at $T = 60$ °C and $h_{rel} \sim 95\%$.

λ (Å)	η	κ (k_BT)	B (MPa)	R (μm)
1.2×10^1	1.8×10^{-2}	17	8.4	1.8

TABLE II. Lamellar periodicity and mechanical properties of deuterated lipids measured at the temperature above the chain melting temperature T_m and $h_{rel} \sim 95\%$.

	T (°C)	d (Å)	κ (k_BT)	B (MPa)
D-Gb3	60	62.6	17	8.4
D-Lac1[a]	80[b]	56.5	32	17
D-Gent[a]	80	50.1	8	21
D-DPPC[c]	60	50.9	18	46

[a]Schneck *et al.* (2008).[19]
[b]Note that T_m of Lac1 lipid is 74 °C.[3]
[c]Schneck *et al.* (2011).[21]

impact of small changes in saccharide chemistry (length and conformation of saccharide head groups) on the mechanics of membranes in a quantitative manner. Since biological studies have identified that sphingolipidoses, such as Fabry disease and Krabbe disease, cause local accumulation of glycolipids, it is of general importance to determine how the accumulation of glycolipids influences the interaction potentials between neighboring membranes. Moreover, as reported by Römer *et al.*,[27] the specific interaction between Gb3 and toxin leads to the formation of highly curved structures, such as lipid nanotubes, suggesting the modulation of membrane mechanics by glycolipids. Therefore, the quantitative determination of mechanical properties of various glycolipid membranes would provide with fundamentals to identify the significance of changes in the expression patterns of glycolipids on membrane mechanics.

Further investigation with the aid of complementary techniques in real space under full hydration, which is closer to biological conditions, would provide more mechanistic insights into the mechanical modulation of biological membranes by local enrichment of glycolipids. For example, to investigate the critical balance between the line tension and bending energy in the tubular membrane invaginations triggered by the specific binding of verotoxin and Shiga toxin to Gb3, quantification of the persistence length of thermally fluctuating membrane tubes being protruded from membrane surfaces observed with the microscope in the absence[46] and the presence[47] of proteins (F-BAR domain proteins) would enable one to gain further insights into the mechanics of highly curved membrane local structures made of glycolipids.

V. CONCLUSIONS

The full deuteration of alkyl chains allowed for quantitative determination of the principal mechanical parameters of Gb3 membranes by means of specular and off-specular neutron scattering. Taking the finite size effect of samples (cut-off radius) into consideration enables the scattering signals to be fully computed from the interacting D-Gb3 membranes in reciprocal space using the membrane displacement correlation function. The best combination of de Gennes parameter λ and Caillé parameter η from the scattering function analysis yields two principal mechanical parameters within the framework of discrete smectic Hamiltonian: the compression modulus B and bending rigidity κ. The obtained results clearly demonstrate the straightforwardness of our strategy, while further investigations into membrane-protein interaction models and asymmetric membrane models would provide a more comprehensive picture of how Gb3 causes changes in the structure and mechanics of cell membranes.

ACKNOWLEDGMENTS

We thank Institut Laue-Langevin for neutron beam time and C. Gege for stimulating discussions. This work was supported by MEXT KAKENHI (Nos. 26247070, 26103521 "Fluctuation and Structures"), EUFP7 "SoftActive," JSPS KAKENHI (No. 26800223), and HeKKSaGOn Consortium. A.Y. thanks E. Schneck for fruitful discussions, A. Makky for help with differential scanning calorimetry measurements, and R. Mandow for help with data analysis. A.R. thanks the Konrad-Adenauer-Stiftung for a Ph.D. scholarship. D.B.W. acknowledges the SFB 803 "Functionality controlled by organization in and between membranes" (Project No. A5), the German Research Foundation (Emmy Noether and Heisenberg Fellowships), and the Fonds der Chemischen Industrie (Dozentenstipendium). A.Y. and A.S.B. are thankful to the Baden-Württemberg State Foundation for the "BWS-plus" scholarship, and A.K. to the Heidelberg Academy of Sciences for supports (WIN Kolleg). A.S.B. thanks the Helmholtz BioInterfaces International Graduate School. M.T. is a member of the German Excellence Cluster "Cell Network" and a Helmholtz Program "BioInterface." The iCeMS is supported by World Premier International Research Center Initiative (WPI), MEXT, Japan.

[1]T. T. Mills, G. E. Toombes, S. Tristram-Nagle, D. M. Smilgies, G. W. Feigenson, and J. F. Nagle, Biophys. J. **95**(2), 669-681 (2008).
[2]J. F. Nagle and S. Tristram-Nagle, Biochim. Biophys. Acta **1469**(3), 159-195 (2000).
[3]M. F. Schneider, R. Zantl, C. Gege, R. R. Schmidt, M. Rappolt, and M. Tanaka, Biophys. J. **84**(1), 306-313 (2003).
[4]B. Demé, M. Dubois, T. Gulik-Krzywicki, and T. Zemb, Langmuir **18**(4), 997-1004 (2001).
[5]J. Pencer, T. Mills, V. Anghel, S. Krueger, R. M. Epand, and J. Katsaras, Eur. Phys. J. E **18**(4), 447-458 (2005).
[6]P. Balgavý, M. Dubničková, N. Kučerka, M. A. Kiselev, S. P. Yaradaikin, and D. Uhríková, Biochim. Biophys. Acta **1512**(1), 40-52 (2001).
[7]G. Pabst, J. Katsaras, and V. Raghunathan, Phys. Rev. Lett. **88**(12), 128101 (2002).
[8]R. P. Rand and V. A. Paesegian, Biochim. Biophys. Acta **988**, 351 (1989).
[9]H. Petrache, N. Gouliaev, S. Tristram-Nagle, R. Zhang, R. Suter, and J. F. Nagle, Phys. Rev. E **57**(6), 7014 (1998).
[10]I. G. Denisov, Y. V. Grinkova, A. A. Lazarides, and S. G. Sligar, J. Am. Chem. Soc. **126**(11), 3477-3487 (2004).
[11]C. R. Safinya, E. B. Sirota, D. Roux, and G. S. Smith, Phys. Rev. Lett. **62**(10), 1134-1137 (1989).
[12]C. R. Safinya, D. Roux, G. S. Smith, S. K. Sinha, P. Dimon, N. A. Clark, and A. M. Bellocq, Phys. Rev. Lett. **57**(21), 2718-2721 (1986).
[13]L. Yang, T. Harroun, W. Heller, T. Weiss, and H. Huang, Biophys. J. **75**, 641 (1998).
[14]K. He, S. Ludtke, D. Worcester, and H. Huang, Biophys. J. **70**, 8 (1996).
[15]T. Salditt, C. Munster, J. Lu, M. Vogel, W. Fenzl, and A. Souvorov, Phys. Rev. E **60**(6), 7285-7289 (1999).
[16]T. Salditt, M. Vogel, and W. Fenzl, Phys. Rev. Lett. **90**(17), 178101 (2003).
[17]H. J. Gabius and S. Gabius, *Glycoscience* (Chapmann & Hall, Weinheim, Germany, 1997).
[18]M. Tanaka, F. Rehfeldt, M. F. Schneider, G. Mathe, A. Albersdorfer, K. R. Neumaier, O. Purrucker, and E. Sackmann, J. Phys.: Condens. Matter **17**(9), S649-S663 (2005).
[19]E. Schneck, F. Rehfeldt, R. G. Oliveira, C. Gege, B. Demé, and M. Tanaka, Phys. Rev. E **78**(6), 061924 (2008).
[20]E. Schneck, R. G. Oliveira, F. Rehfeldt, B. Demé, K. Brandenburg, U. Seydel, and M. Tanaka, Phys. Rev. E **80**(4), 041929 (2009).
[21]E. Schneck, B. Demé, C. Gege, and M. Tanaka, Biophys. J. **100**(9), 2151-2159 (2011).
[22]N. Lei, C. R. Safinya, and R. F. Bruinsma, J. Phys. II **5**(8), 1155-1163 (1995).
[23]C. A. Lingwood, H. Law, S. Richardson, M. Petric, J. L. Brunton, S. De Grandis, and M. Karmali, J. Biol. Chem. **262**, 8834 (1987).
[24]A. A. Lindberg, J. E. Brown, N. Strömberg, M. Westling-Ryd, J. E. Schultz, and K. A. Karlsson, J. Biol. Chem. **262**, 1785 (1987).
[25]H. Isobe, K. Cho, N. Solin, D. B. Werz, P. H. Seeberger, and E. Nakamura, Org. Lett. **9**(22), 4611-4614 (2007).
[26]M. A. Karmali, M. Petric, C. Lim, P. C. Fleming, G. S. Arbus, and H. Lior, J. Infect. Dis. **151**(5), 775-782 (1985).
[27]W. Römer, L. Berland, V. Chambon, K. Gaus, B. Windschiegl, D. Tenza, M. R. Aly, V. Fraisier, J. C. Florent, D. Perrais, C. Lamaze, G. Raposo, C. Steinem, P. Sens, P. Bassereau, and L. Johannes, Nature **450**(7170), 670-675 (2007).

[28]R. J. Desnick, Y. A. Ioannou, and C. M. Eng, in *The Metabolic Molecular Bases of Inherited Disease*, edited by C. R. Scriver, A. L. Beaudet, W. S. Sly, and D. Valle (McGraw-Hill, 1995), Vol. II, pp. 2741-2784.
[29]H. Askari, C. R. Kaneski, C. Semino-Mora, P. Desai, A. Ang, D. E. Kleiner, L. T. Perlee, M. Quezado, L. E. Spollen, B. A. Wustman, and R. Schiffmann, Virchows Arch. **451**(4), 823-834 (2007).
[30]E. A. Evans and P. L. La Celle, Blood **45**, 29 (1975).
[31]F. Brochard and J. F. Lennon, J. Phys. (Paris) **36**(11), 1035-1047 (1975).
[32]X. Zhu and R. R. Schmidt, Angew. Chem., Int. Ed. Engl. **48**(11), 1900-1934 (2009).
[33]F. Bosse, L. A. Marcaurelle, and P. H. Seeberger, J. Org. Chem. **67**(19), 6659-6670 (2002).
[34]D. B. Werz, B. Castagner, and P. H. Seeberger, J. Am. Chem. Soc. **129**(10), 2770-2771 (2007).
[35]O. M. Schütte, A. Ries, A. Orth, L. J. Patalag, W. Römer, C. Steinem, and D. B. Werz, Chem. Sci. **5**, 3104 (2014).
[36]G. Zemplén and E. Pacsu, Ber. Dtsch. Chem. Ges. (A and B Ser.) **62**(6), 1613 (1929).
[37]See http://www.ill.eu/instruments-support/instruments-groups/instruments/d16/.
[38]W. Kern and D. A. Puotinen, RCA Rev. **31**, 187 (1970).
[39]See supplementary material at http://dx.doi.org/10.1063/1.4918585 for the details of the synthesis and the scattering intensity measured in each condition.
[40]L. Landau and E. Lifshitz, *Statistical Physics, Part 1* (Butterworth-Heinemann, Oxford, 1980), Vol. 5.
[41]B. V. Derjaguin, N. V. Churaev, V. M. Muller, and J. A. Kitchener, *Surface Forces* (Springer, 1987).
[42]J. Als-Nielsen and D. McMorrow, *Elements of Modern X-Ray Physics* (John Wiley & Sons, 2011).
[43]S. K. Sinha, Phys. III (Les Ulis) **4**(9), 1543-1557 (1994).
[44]B. Deme, M. Dubois, and T. Zemb, Biophys. J. **82**(1), 215-225 (2002).
[45]J. N. Israelachvili, *Intermolecular and Surface Forces* (Academic Press, London, San Diego, 1991).
[46]A. Yamamoto and M. Ichikawa, Phys. Rev. E **86**(6), 061905 (2012).
[47]Y. Tanaka-Takiguchi, T. Itoh, K. Tsujita, S. Yamada, M. Yanagisawa, K. Fujiwara, A. Yamamoto, M. Ichikawa, and K. Takiguchi, Langmuir **29**(1), 328-336 (2013).
[48]This treatment is valid due to the close correlation between Γ and q_z.
[49]Due to the suppression of Landau-Peierls instability,[12,15] the width of specular peak does not reflect the number of vertically correlated membranes but the instrument resolution along q_z.
[50]The integrated intensity of Bragg sheet depends on only the membrane self-correlation function $g_0(r)$, whereas the sheet width of the Bragg sheets along q_z depends on only λ.[16]
[51]Since the intensity is high only near the Bragg sheet, the integration range can be reduced as indicated in Fig. 5(c) (broken line).[15]